Influence of Ligands on the Dynamics of Hydrogen Elimination in Cationic Complexes of Co and Rh†

Rong Xu, Maik Bittner, Günter Klatt, and Horst Köppel*

Theoretische Chemie, Physikalisch-Chemisches Institut, Universität Heidelberg, Im Neuenheimer Feld 229, 69120 Heidelberg, Germany

Received: August 28, 2008

The quantum dynamics of β-hydrogen elimination in cationic transition metal complexes $[CpML(C_2H_4)H]^+$ (M = Co, Rh; L = PH_3, PF_3, PMe_3, $P(OMe)_3$) is studied theoretically. The underlying potential energy profiles are obtained at the DFT level of theory; the nuclear motion is computed by the method of wave packet propagation (i.e., by integrating the time-dependent Schrödinger equation). For the Co as well as the Rh complexes, agostic intermediates relevant to the insertion/elimination process exist. Complexes containing each ligand are studied for both transition metals from an electronic structure point of view and, in addition, the ligand influence on the dynamics is compared. The results allow us to draw conclusions concerning the influence of the energetics as well as the different masses on vibrational periods and lifetimes of these complexes due to β-elimination.

1. Introduction

In 1995 the activity of diimine complexes of Ni and Pd in ethylene polymerization was discovered by Brookhart and co-workers.[1] Much attention has since been paid to olefin polymerization using late transition metal catalysts (see, for example, ref 2 and references therein). Compared to early transition metals, they provide access to polymers with novel branching structures and therefore new physical properties. They also exhibit less oxophilicity and therefore a greater tolerance toward polar reagents. Previous studies have indicated that the catalytic cycle follows the Cossee−Arlmann mechanism, starting with olefin coordination at the metal and subsequent insertion of the olefin into the metal−carbon bond of the polymer chain (see, e.g., refs 3 and 4). To shed more light on the mechanistic details of the reaction, we have studied the initial reaction of ethylene with hydrido complexes of the late transition metals Co and Rh and found that at least five stationary points (three local minima and two interconnecting transition states) are involved.[5] This is schematically represented in Figure 1, where the reaction sequence from the ethylene complex **1** to the ethyl complex **3** corresponds to olefin insertion, i.e., the propagation of the polymer chain. The reverse sequence is known as β-elimination and is expected to be important in systems for which the TS1 barrier is low compared to the activation energy associated with TS2, as is the case for late transition metal catalysts. It is well-known from experiment (mostly through the work of Brookhart and co-workers[2,6−9]) that late transition metal complexes indeed exhibit fast hydrogen elimination and reinsertion, leading to branched and hyperbranched products in olefin polymerization; agostic intermediates analogous to **2** play a role in the insertion process. Since β-elimination may result in either branching of the polymer chain or chain transfer, i.e., termination of the polymerization with an associated yield of polymer with low molecular weight, a better understanding of this hydrogen transfer reaction is key to designing catalysts tailored to a given purpose. Moreover, the aforementioned olefin insertion/hydrogen elimination reactions constitute important steps in a number of catalytic reaction cycles, for example, hydrogenation and hydroformylation.

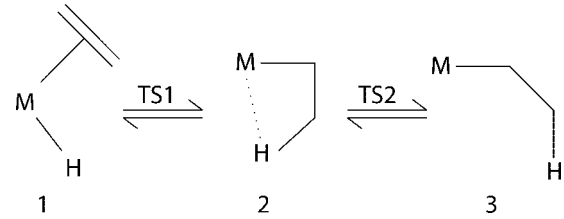

Figure 1. Schematic representation of the migratory insertion (from the ethylene complex **1** to the ethyl complex **3**, and the β -elimination (from **3** to **1**), together with the agostic intermediate **2** and the interconnecting transition states TS1 and TS2.

A number of theoretical investigations of these processes have become available,[10−18] which focus on structural and energetic quantities pertaining to, for example, the calculation of rate constants within the usual framework of transition state theory (TST). The dynamics in these systems is often studied within a classical framework.[19,20] However, quantum effects like zero-point energy and tunneling may have a significant influence on the nuclear motion. This applies especially to the motion of light atoms, as in the case of hydrogen transfer. These phenomena may also have a noticeable effect on thermal rate constants. For these reasons, we have recently initiated a new line of research investigating the quantum dynamics of the aforementioned olefin insertion and hydrogen elimination processes. This enabled us to determine time constants for the motion along the reaction path, as well as lifetimes arising from hydrogen elimination, for two cationic Co and Rh complexes for the first time.[5] While this initial study was based on the quantum dynamics on a one-dimensional reaction path following a Franck−Condon (FC) type excitation, this treatment has subsequently been extended to two and three nuclear degrees of freedom, and their interplay with the motion along the reaction coordinate has been established.[21]

† Part of the "Sason S. Shaik Festschrift".

* Corresponding author. Telephone: +49 (6221) 54 52 14. Fax: +49 (6221) 54 52 21. E-mail: horst.koeppel@pci.uni-heidelberg.de.

10.1021/jp807676n CCC: $40.75
Published on Web 10/28/2008

In the present study of the β-elimination/olefin insertion reaction for the late transition metal complexes $[CpML(C_2H_4)H]^+$ (M = Co, Rh; L = PH_3, PF_3, PMe_3, $P(OMe)_3$), we compare the influence of different phosphine ligands L and metal atoms M on the energetics and dynamics of the reaction sequence. It should be mentioned that the case L = PH_3 has been treated in our earlier work and is included here for comparison. The analogous complex $[C_5Me_5CoHP(OMe)_3]^+$ is known to be an active catalyst for the living poymerization of ethylene.[22] Ligands with different donor/acceptor properties were chosen in order to enable us to detect a possible influence of the charge at the transition metal on the energetics and nuclear dynamics. The use of both electronic structure calculations (for the determination of the relative energies of the various relevant species, as well as the resulting energetic barriers and potential energy profiles) and wave packet propagation methods permits us to compare results from TST with predictions from quantum molecular dynamics. We propose guidelines for the selection of ligands that minimize the occurrence of β-elimination and suggest a method to compare prospective ligands on the basis of the photoelectron spectra (PES) of their complexes.

The paper is organized as follows. In section 2, we describe in detail the computational methods employed for our electronic structure work, as well as the methods used in our quantum dynamical simulations. The results for the various stationary points and potential energy profiles of the systems are presented and discussed in section 3. The corresponding dynamical data and their interpretation follow in section 4. Finally, section 5 concludes with a summary and perspectives for future work.

2. Computational Methods

2.1. Electronic Structure Calculations. The electronic structure calculations of this work comprise geometry optimizations, harmonic frequency calculations plus thermochemistry analysis, and intrinsic reaction coordinate (IRC) calculations. All electronic structure calculations were carried out by using the DFT method and the BP86 functional[23−25] with the same split basis as used in our previous work.[5] This split basis is composed of the standard SDD and 6-31G** basis sets. In this basis, the transition metal is treated with the SDD basis; active hydrogens (i.e., terminal hydrogen atoms at the β-carbon in the ethylene moiety and the migrating hydrogen atom), phosphorus, and carbon are treated with the 6-31G** basis set, and the nonactive hydrogen atoms are treated with 6-31G*. The reliability of this compromise has been proven by our previous work.[5]

The geometries of all stationary points involved were fully optimized. To localize the transition states, a combined scanning and transit-guided quasi-Newton (STQN) approach was used.[26] All stationary points were characterized as minima or transition states by vibrational analysis. Transition states were verified as having only one imaginary frequency. All DFT calculations were performed using the Gaussian 03 program package.[27]

An important part of our electronic structure computations for this work was the determination of the reaction-path energy profile. The intrinsic reaction coordinate (IRC) method[28−31] was used for this purpose. With the IRC method, a reaction path was computed with respect to a mass-weighted coordinate x. The reaction coordinate reflects how much and how many atoms are moving between two points along the curve.

As the IRC method requires, we started calculations from the transition states involved in the migratory insertion reaction. The reaction path was followed in both forward and reverse directions. Starting from the initial transition state geometry, the geometry was optimized at each point along the reaction path. The reaction path segment between any two adjacent points is described by an arc of a circle, so that the gradients at the end points of the arc are tangent to the path. The IRC calculation step size should be small enough to obtain a complete, smooth, and accurate reaction path energy profile. For this reason, we used a step size of 0.1−0.3 (amu$^{1/2}$ bohr), resulting in a total number of 1000−2000 optimization points for the entire reaction path. In this manner, we computed reaction-path energy profiles for all transition metal complexes studied here.

2.2. Quantum Dynamical Simulations. In this work, a wave packet propagation method is used for our quantum dynamical simulations.[32−35] The time-dependent Schrödinger equation for the nuclear motion is solved explicitly. Here, we mostly deal with one-dimensional quantum dynamic simulations, namely, a wave packet propagation along the mass-weighted reaction path. The reaction-path potential and the wave packet are represented on a one-dimensional grid.

Our original grid, obtained from the IRC calculation, ranges from the ethylene to the ethyl minimum. It is extended in both directions to allow for the description of a "stable" ethyl structure as well as complex dissociation.

The dynamics of the nuclear motion is governed by an effective Hamiltonian of the form

$$\mathscr{H} = -\frac{\hbar^2}{2}\frac{\partial^2}{\partial x^2} + V(x) + V_{CAP}(x) \qquad (1)$$

V_{CAP} is a complex absorbing potential (CAP),[36−39] which extends the IRC potential on the ethylene side. It is included not only to prevent unphysical reflections and wraparounds but also to simulate the decay of the complexes once the wave packet reaches the grid boundary at the ethylene minimum. This corresponds to dissociation of the ethylene structure and thus to the decay of the complex due to β-elimination.

Our V_{CAP} has the form

$$V_{CAP}(x) = -i\eta(x - x_0)^2 \quad \text{for} \quad x \le x_0 \qquad (2)$$

where η is the strength parameter and x_0 is the starting point of the CAP. The parameters were chosen to meet the requirements of no reflection and no transmission of an incoming wave packet. They can be obtained by monitoring the energy of the ground state, the lifetime of the state, and the total time-dependent norm of the wave packet as a function of η and x_0. In this work, η is chosen to be 5×10^{-8} a.u. and x_0 is equal to the mass-weighted coordinate ranging from −160 to −15 ($m_e^{1/2}a_0$) of the ethylene minimum on the IRC curve. This is defined in relation to the mass-weighted coordinate of the first transition state TS1, for which we define $x = 0$. Furthermore, we choose the left terminal point of our grid to be $x = -500$ ($m_e^{1/2}a_0$).

If a wave packet reaches the other end of the reaction path potential (i.e., the ethyl minimum; see Figure 4), it can form a stable solution in this region, or if its energy is high enough, it can tunnel back through the barrier and isomerize to the agostic structure. Therefore, we decided to extrapolate the potential at this end by a real harmonic function, which has the form

$$V(x) = \mu(x - x_1)^2 \quad \text{for} \quad x \ge x_1 \qquad (3)$$

where μ is the force constant and x_1 is the position of the minimum. For each of the complexes examined, we fitted this continuation to be approximately symmetric with respect to the respective ethyl minima. For example, for the Rh−PH_3 complex, the parameters in eq 3 are $\mu = 5 \times 10^{-8}$ a.u. and $x_1 = 1262.6$

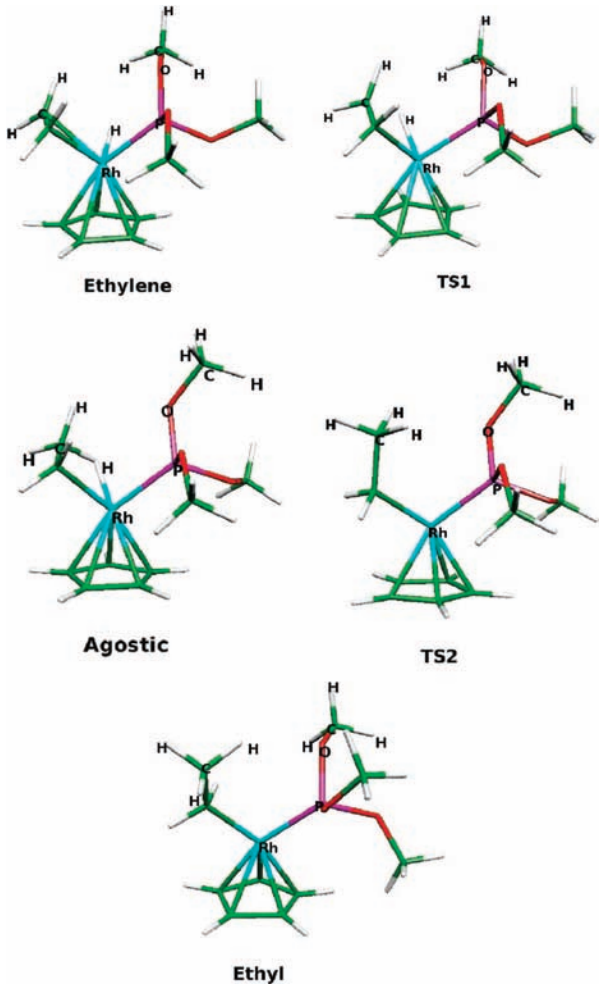

Figure 2. Structures corresponding to stationary points relvant to the ethylene insertion/β-elimination process for the [CpRhP(OMe)$_3$-H(C$_2$H$_4$)]$^+$ complex.

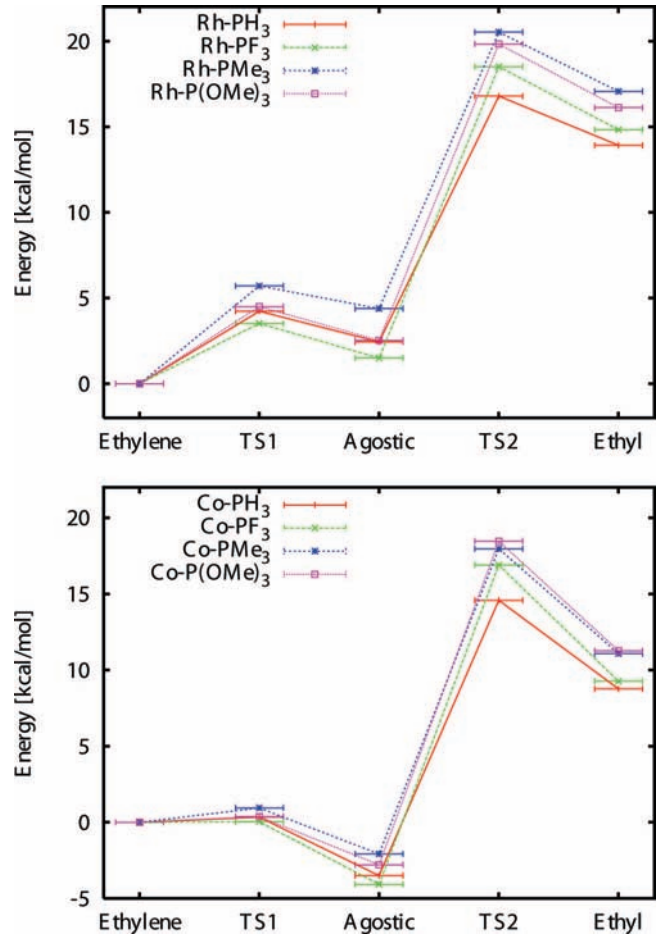

Figure 3. Relative electronic energies (without ZPE) for the [CpMLH(C$_2$H$_4$)]$^+$ complexes. The energy of the ethylene structure is always set to zero. The other energies are defined in relation to the ethylene structure.

$m_e^{1/2}a_0$. The resulting real parts of the potential are included in Figure 4 at the right-hand side.

On the basis of eq 1, a time-dependent wave packet describing the nuclear motion can be obtained by solving the corresponding time-dependent Schrödinger equation. The solution is obtained by the Lanczos−Arnoldi algorithm (LA),[40,41] which is suitable for non-Hermitian operators.

The wave packets have been propagated for 2048 fs with time steps of 0.5 fs and a Lanczos order of 30. For all Rh complexes as well as Co−PMe$_3$, the starting positions of the initial wave packets are the reaction coordinates of the first transition state TS1 (0.0 $m_e^{1/2}a_0$) or the second transition state TS2 (e.g., 973 $m_e^{1/2}a_0$ for the Rh−PH$_3$ parent complex). For the remaining Co complexes, the TS1 barrier disappeared when the energies were corrected for zero point energy (see section 3.2). We therefore selected the coordinates corresponding to the respective ethylene structure (ES) as starting positions instead.

The widths of these initial wave packets $\Delta\Psi(0)$ were set to the widths of suitable harmonic oscillator ground-state wave functions. The force constants for these harmonic oscillators are approximately defined by the curvatures of the inverse potentials formed by the energetic barriers at TS1 and TS2. The resulting widths for the Rh−PH$_3$ complex are 17 $m_e^{1/2}a_0$ (TS1) and 50 $m_e^{1/2}a_0$ (TS2). We proceeded to vary $\Delta\Psi(0)$ for the remaining complexes and found that our results did not change significantly. Therefore, we assigned these widths also to the initial wave packets for the other complexes investigated in our study. The software used for the wave packet propagation was developed in our group and tested for the vinylidene−acetylene isomerization reaction.[32]

The spectra are calculated by a fast Fourier transform (FFT) of the overlap of the initial wave packet $|\psi_0\rangle$ and a time-developed one, $\exp(-i\mathcal{H}t)|\psi_0\rangle$ (autocorrelation function $C(t)$):

$$C(t) = \langle\psi_0|e^{-(i/\hbar)\mathcal{H}t}|\psi_0\rangle \tag{4}$$

The spectrum is thus given by[42]

$$P(E) = \frac{1}{2\pi}\int_{-\infty}^{\infty} C(t)e^{(i/\hbar)Et}\,dt \tag{5}$$

From the nonhermitian Hamilton operator $\mathcal{H}$, complex energy eigenvalues E_i are obtained. These are extracted with a filter diagonalization scheme using a box filter.[43−46] Their real parts give directly the positions of the peaks in the FFT spectrum. These are used to calculate the oscillation frequency of the time-dependent wave function within the potential. The imaginary parts are the lifetimes of the corresponding metastable states.

The norm of a time-dependent wave packet describes its decay.

$$N(t) = \langle\psi(t)|\psi(t)\rangle \tag{6}$$

To extract the relevant time constants, it can be fitted to the following formula:

$$y = (1 - c)e^{-t/\tau} + c \quad (7)$$

Here, τ represents the lifetime, and the parameter c corresponds to the value of the norm at the terminal propagation time. As a consequence, on the basis of the fitted norm curve, the lifetime of a wave packet can be determined.

3. Electronic Structure Calculations

3.1. Energies of Selected Stationary Points. Following our previous study of the phosphine parent complexes,[5] we expected the β-hydrogen elimination/insertion in $[CpMLH(C_2H_4)]^+$ complexes to involve at least five stationary points: three minimum energy conformations corresponding to an ethylene hydride, an agostic (η^2-ethyl), and an η^1-ethyl structure, and two transition states TS1 and TS2 interconnecting them. Figure 2 displays the structures corresponding to these stationary points for the L = $P(OMe)_3$ complex. The variation of the potential energy for the various stationary points is indicated in Figure 3, and the potential energies corrected for zero-point energy (ZPE) are summarized in Table 1.

It is evident that the ethylene structures represent global minima for the Rh complexes, while the agostic structures are global minima for the Co complexes; they are thus resting states of the corresponding catalysts. This result is in agreement with experimental data[7] and previous DFT results.[14,47]

Figure 3 of the uncorrected electronic energies appears to confirm that the migratory insertion reaction indeed proceeds in two steps for all complexes, i.e., an initial migration step that converts the ethylene structure into the agostic structure via transition state TS1 and the subsequent transformation of the agostic structure to the ethyl structure via transition state TS2.

Once the effect of ZPE is included (Table 1), it becomes evident that this assumption does not hold for all ligands examined; in particular we note that the agostic minimum disappears for the Rh−PMe_3 complex, and the TS1 barrier vanishes for all Co complexes except Co−PMe_3 (see subsection 3.2).

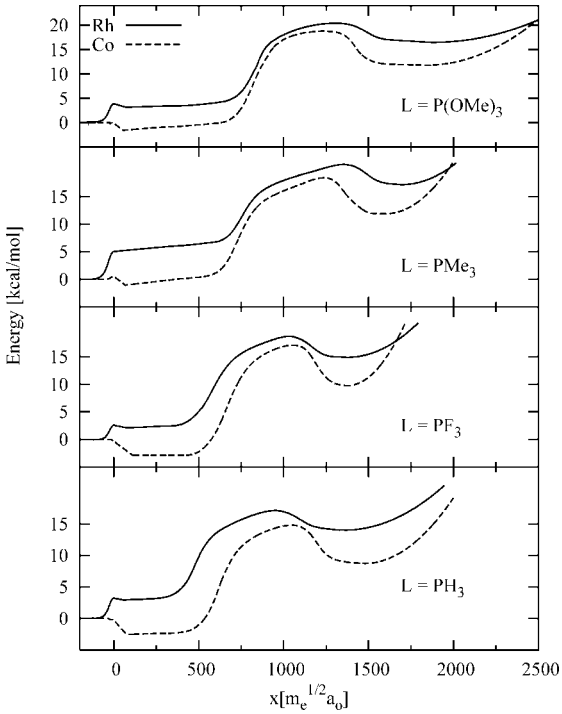

Figure 4. ZPE-corrected potential energy curves along the reaction path in mass-weighted intrinsic coordinates for the complexes $[CpMLH(C_2H_4)]^+$.

The barrier to β-elimination is the energy difference

$$\Delta E_1 = E_{TS1/ES} - E_{agostic} \quad (8)$$

On comparison of these energy differences in Table 1, it is seen that the barriers for the Co complexes are more than twice as high as those for any of the Rh complexes; cobalt polymerization catalysts are therefore expected to exhibit less β-elimination and thus generate polymer of higher molecular weight and with less branching. If the phosphine ligands for the Co complexes are ordered according to barrier height, the following series is obtained:

$$PMe_3 \approx P(OMe)_3 < PH_3 < PF_3$$

Transition state theory thus predicts that the importance of β-elimination should diminish in the same order and identifies PF_3 as the ligand conferring the greatest stability to the agostic intermediate. The relative energy barrier for the β-elimination step of the Co complexes increases approximately in the same order as the electron acceptor strength of the ligand. For the Rh complexes, the analogous ligand order is found to be $PMe_3 < PH_3 < PF_3 < P(OMe)_3$. The correlation with the ligand donor/acceptor strength is less clear in this case, but it is noteworthy nevertheless that the lowest ΔE_1 values for both metals occur for the strong donor PMe_3, even becoming negative for the rhodium complex. No agostic intermediate therefore exists for Rh−PMe_3.

The second insertion reaction step corresponds to the transformation of the agostic structure to the ethyl structure via transition state TS2. The relative energy barrier for this reaction step is much higher than that for the first migratory step. For the Rh complexes the relative energy barrier in this step increases in the order of the ligands $PH_3 < PF_3 < P(OMe)_3 < PMe_3$, and for the Co complexes in the order of the ligands $PH_3 < PF_3 < PMe_3 < P(OMe)_3$, which is the same series as arranged by ligand size. This result indicates that the steric effect of L has a substantial influence on the energy barrier of this reaction step, whereas the electronic effect of the ligand plays a less important role. The steric effect of the ligand L is larger for the Co complexes than for the Rh complexes, because the effect depends on the steric hindrance caused by L, which increases with decreasing M−L distance. A more detailed discussion of these issues (energetic and structural aspects) is beyond the scope of this work and will be published separately.[48]

3.2. Reaction-Path Energy Curves. The reaction-path energy curves in Figure 4 consist of three sections. The first two parts correspond to results from IRC calculations with starting points TS1 and TS2, respectively. These are subsequently modified by adding estimated ZPEs, which have been calculated

TABLE 1: Energies in kcal/mol of Selected Conformations for the Complexes $[CpMLH(C_2H_4)]^+$[a]

M	L	ethylene	TS1	agostic	TS2	ethyl	ΔE_1	ΔE_2
Rh	PH_3	0.0	3.21	2.90	17.14	14.02	0.3	3.1
	PF_3	0.0	2.61	2.10	18.83	14.84	0.5	4.0
	PMe_3	0.0	5.04	5.13	20.83	17.15	−0.1	3.7
	$P(OMe)_3$	0.0	3.81	3.14	20.40	16.14	0.7	4.3
Co	PH_3	0.0	−0.24	−2.50	14.82	8.73	2.5	6.1
	PF_3	0.0	−0.35	−2.85	17.05	9.76	2.9	7.3
	PMe_3	0.0	0.52	−1.05	18.39	11.47	1.6	6.9
	$P(OMe)_3$	0.0	−0.15	−1.59	18.75	11.50	1.6	7.3

[a] The conformations are defined in Figure 2. The energies are given in relation to the respective ethylene conformations, which define the zero of energy. The energy barriers ΔE_1 and ΔE_2 discussed in Chapters 3 and 4 are also included.

from the ZPEs of the adjacent stationary points using a linear interpolation scheme. The third section is obtained by a harmonic extrapolation of the section between TS2 and x_1.

The IRC curves provide a direct and convenient way to probe the change of the energy and the structure of the complex along the reaction path. Consequently, the reaction sequence can be deduced from an analysis of the IRC curves. Inspection of Figure 4 indicates that the energetic features discussed above for Figure 3 no longer hold for all of the ZPE-corrected IRC curves. In particular, not all the stationary points mentioned previously can be identified on all curves. With the exception of complexes with the electron-rich PMe_3 ligand, we observe that for the Rh complexes TS1 corresponds to a narrow barrier, while for the Co complexes this barrier completely disappears after the ZPE correction is applied. This indicates that, from a energetic point of view, the first part of the migratory insertion (from the ethylene to the agostic conformation) is very fast for these complexes and should be easily observed at room temperature. Interestingly, the IRC curve for the Rh−PMe_3 complex is characterized by the absence of an agostic minimum, which would indicate that this compound might be least effective as a polymerization catalyst. In contrast, the analogous Co complex is the only one for which a small TS1 barrier is observed. For the second transition state TS2 we find a much broader and higher barrier for all complexes of both transition metals. We also inspected the structure of the ligand L for changes during the reaction but found little.[48] This suggests that the electronic and steric effects of L hardly change during this process.

4. Quantum Dynamical Results

As mentioned above, we use a wave packet propagation method for the quantum dynamical simulation. Since our main purpose is to simulate the β-hydrogen elimination reaction for the transition metal complexes involved, one-dimensional quantum dynamical calculations were carried out using the aforementioned reaction path energy curves and TS1/ES or TS2 as the respective starting point. Experimentally, this corresponds to a nonvertical or non-Franck−Condon (non-FC) transition from the equilibrium structure of the neutral precursor complex and could be achieved by broadband excitation with suitably shaped femtosecond laser pulses.[49−51]

4.1. Wave-Packet Propagation. Figure 5 displays the time-dependent wave functions (with starting points TS1 and ES, respectively) for the Rh−PF_3 and the Co−PF_3 complexes.

Inspecting Figure 5a, we can analyze in detail the behavior of the time-dependent wave packet. After starting its propagation from TS1, it separates into two parts in rather short time. One part propagates to the left of the barrier formed by TS1 and moves toward the ethylene minimum. This part of the packet represents the molecules which are isomerizing to the ethylene complex. It will be absorbed by the CAP after it has passed through the ethylene minimum (i.e., for $x < x_0$). Therefore, this part of the wave packet describes the elimination of ethylene from the complex.

The other part of the wave packet, which propagates toward the right-hand side of the barrier formed by TS1, moves into the potential energy well of the agostic minimum, where it starts to oscillate. During each oscillation period this wave packet evolves from the TS1 barrier toward the region of TS2, where it is reflected. It then proceeds back to the TS1 barrier whereupon a part of the packet penetrates the barrier and subsequently evolves toward the ethylene minimum and is absorbed by the CAP. The rest of the packet continues to oscillate in the agostic minimum. Each time the packet

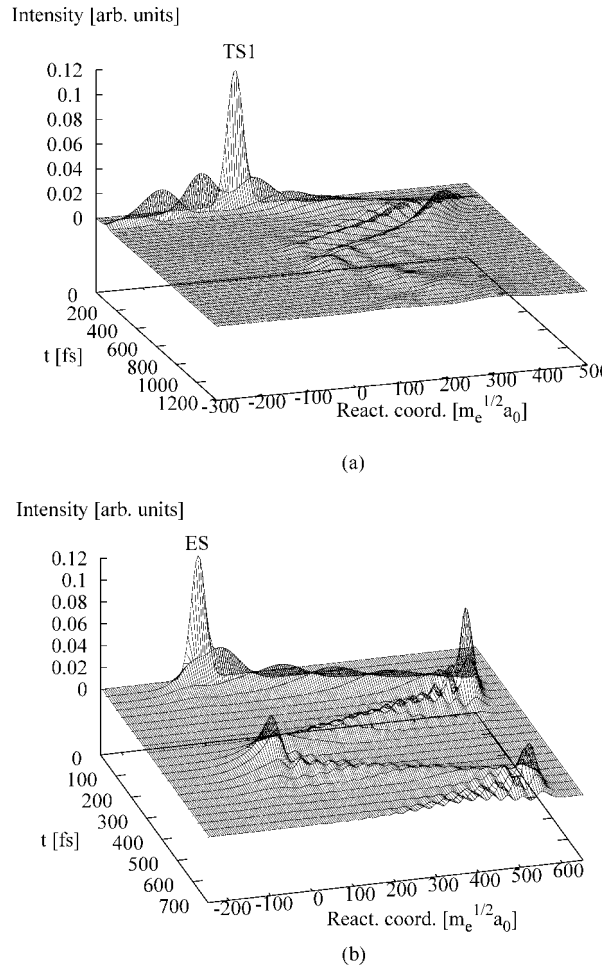

Figure 5. Oscillation of the time-dependent wave function along the reaction coordinate for (a) $[CpRhPF_3H(C_2H_4)]^+$ and (b) $[CpCoPF_3H(C_2H_4)]^+$. TS1 and ES were selected as the starting points for the respective propagations.

completes an oscillation and reaches the TS1 barrier, a part of the packet overcomes the barrier and is absorbed by the CAP. As time increases, a larger and larger part of the wave packet is absorbed. This reflects the increasing probability for the Rh complexes to undergo the elimination process.

Figure 5b shows that the wave packet representing the Co complex undergoes a similar propagation. The part of the wave packet initially moving to the right ends up oscillating in the agostic minimum region in a similar way as described above. However, it is noticed that the intensity of the wave packet decays slower in comparison to the Rh complex. This indicates that the elimination process for the Co complex should be slower than that for the Rh complex.

If the initial wave packet is located at the transition state TS2, a similar behavior of the time-dependent wave packet can be observed. Again, the wave packet is split into two parts at the start of the propagation. One part of the packet evolves and oscillates in the agostic minimum in the same way as described for Figure 5a. In contrast to the previous situation, the other part of the packet now moves into the ethyl minimum and oscillates there. At regular intervals, a part of that wave packet crosses the TS2 barrier, from which it proceeds to overcome the TS1 barrier and is absorbed by the CAP. This suggests that the elimination reaction for a transition metal complex would proceed more slowly if its initial structure is prepared at TS2.

For all transition metal complexes involved in this work, we inspected and observed the overall process of a wave packet

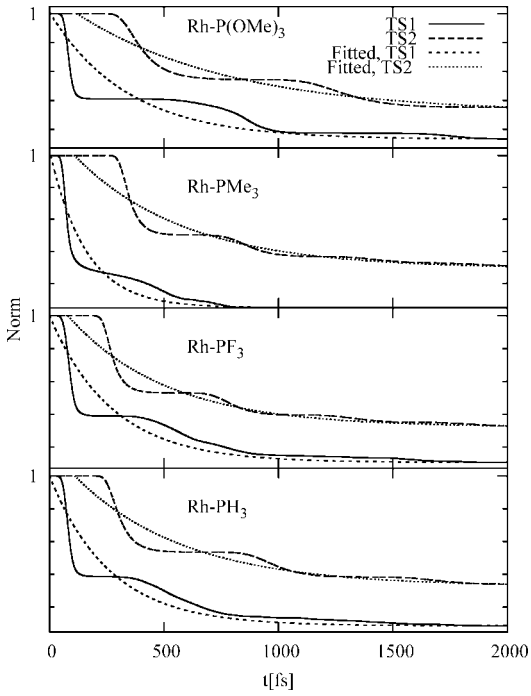

Figure 6. Time evolution of the norm for one-dimensional wave packets starting at TS1 or TS2 for the $[CpRhLH(C_2H_4)]^+$ complexes. The fitted norm is based on $y = (1 - c)e^{-t/\tau} + c$.

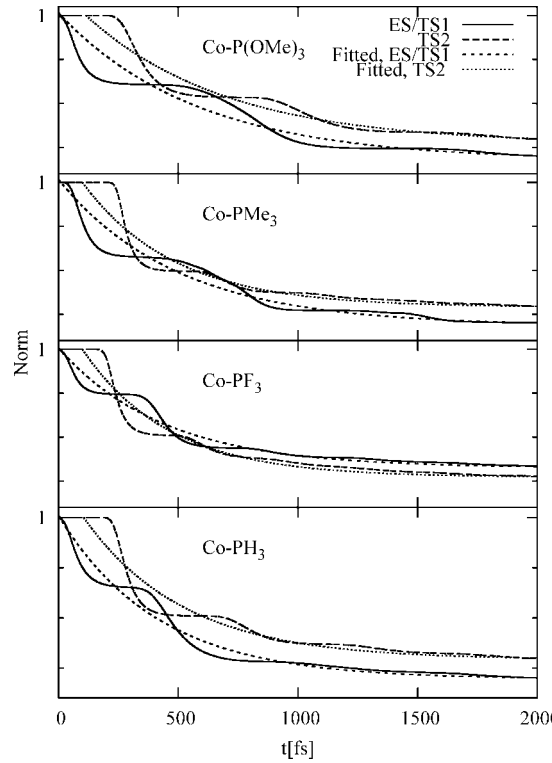

Figure 7. Time evolution of the norm for one-dimensional wave packets starting at ES (TS1 for L = PMe_3) and TS2 for the $[CpCoLH(C_2H_4)]^+$ complexes. The fitted norm is based on $y = (1 - c)e^{-t/\tau} + c$.

propagating along the respective IRC energy curves. The results show that the time-dependent wave packets for these complexes undergo similar oscillations.[5,21] In order to understand the wave packet propagation at a more fundamental level, it is necessary to describe the overall process quantitatively.

4.2. Norm of the Time-Dependent Wave Packet. The overall progress of a wave packet propagation can be monitored by plotting the norm $N(t)$ of the wave function as a function of time. Figures 6 and 7 present time evolutions of the norms of respective wave packets starting at TS1/ES and TS2 for all transition metal complexes investigated. An exponential fit of the norm according to eq 7 is also plotted.

As shown in Figure 6, the norm of the wave packet at the beginning of each propagation is set to 1. The norm then decreases in a stepwise fashion over time. The steps are nearly equidistant, with the distance corresponding to an oscillation period of the wave packet moving in the respective minimum region (agostic for the initial wave packet located at TS1/ES, ethyl for the initial wave packet located at TS2). The steep sections of $N(t)$ correspond to the absorption of that part of the wave packet that has penetrated the region of the TS1 barrier and moved into the CAP region. Consequently, the oscillation period could be obtained by inspecting the time evolution of the norm. For instance, for a wave packet originating at TS2 for the ethyl minimum of the $Rh-PF_3$ complex, it is thus estimated to be 430 fs, and this value is close to that found by tracing the wave packet (454 fs). However, in most cases we were unable to identify the steps of the norm decay accurately. We therefore decided to determine the oscillation period by tracing the position of the wave packet maximum. Table 2 summarizes the oscillation periods of the time-dependent wave packets for the transition metal complexes studied here. T_1 and T_2 represent the oscillation periods in the agostic and ethyl minima, respectively.

Since the oscillation periods T are inversely proportional to the level spacing in a photoelectron spectrum (PES) corresponding to an excitation to either TS1/ES or TS2, they can in principle be measured experimentally. To our knowledge, no such spectrum has been measured so far. We will discuss this subject in detail in subsection 4.3.

TABLE 2: Oscillation Periods, T, and Lifetimes, τ (in fs), for the complexes $[CpMLH(C_2H_4)]^+$ of $[CpMLH(C_2H_4)]^+$ (M = Rh, Co) (L = PH_3, PF_3, PMe_3, $P(OMe)_3$) for Wave Packets Starting at TS1 (ES for all Co Complexes Except Co−PMe_3) or TS2

M	L	τ_1	τ_2	T_1	T_2
Rh	PH_3	263	479	640	600
	PF_3	272	430	700	454
	PMe_3	156	487	636	470
	$P(OMe)_3$	332	640	810	682
Co	PH_3	414	418	410	460
	PF_3	439	360	416	310
	PMe_3	496	383	680	360
	$P(OMe)_3$	577	586	790	600

Table 2 shows that, for each ligand L, the oscillation period T_1 for the Rh complex is longer than the corresponding time for the Co complex. This is because the higher ΔE_1 values for the Co complex will result in faster propagation in the agostic potential well and hence a shorter oscillation period. For a harmonic potential

$$T = 2\pi\sqrt{m/k} \tag{9}$$

where k represents the curvature or "steepness" of the harmonic potential or, more generally, the average of the second derivative of the potential over the agostic minimum region. Higher ΔE_1 values correspond to steeper wells and therefore lower T values, while higher masses m increase the oscillation period.

Since the ΔE_1 values do not drastically differ among the Co complexes, we find in accordance with eq 9 that their oscillation periods T_1 increase in line with ligand mass:

$$PH_3 < PF_3 < PMe_3 < P(OMe)_3$$

Except for L = PMe_3, this correlation also holds for the Rh complexes. The short oscillation time for the trimethylphosphine ligand is due to its lack of an agostic minimum; instead of a genuine oscillation, one therefore observes a complete decay of the norm after two absorption steps for this system. T_1 would therefore perhaps more fittingly be termed "reflection time" in this case.

From Figures 6 and 7, it is seen that the "decay" of the norm of a wave packet is almost complete after the first few oscillation periods. This process can be ascribed to the decay of the respective complex due to H-elimination following broadband excitation to TS1/ES or TS2. As mentioned in section 2, the lifetime of the system can be determined by fitting an exponential decay function to the norm. All lifetimes obtained from the wave packets for all transition metal complexes are summarized in Table 2. Here, τ_1 and τ_2 represent the lifetimes of wave packets starting at TS1/ES and TS2, respectively. We consider τ_1 an indicator for the stability of the catalyst's agostic state against β-elimination.

When the lifetimes of different ligands are compared for the same transition metal, it is found that τ_1 increases in parallel with T_1, i.e., a ligand with a longer oscillation time will also increase the lifetime of a particular complex. However, for identical ligands L, the lifetimes for the Co complexes are longer than those for the Rh complexes. This is a consequence of the considerably lower energies (by over 2 kcal/mol) of the wave packet starting points at ES/TS1 for M = Co, resulting in a slower propagation in the region of the ethylene structure and the CAP.

Our quantum dynamical results demonstrate that the broadband excitation lifetime and hence the stability against β-elimination are influenced by the dynamics in both the agostic region and the ethylene region. For any particular ligand, cobalt catalysts are expected to generate polymer that is characterized by higher molecular weight and less branching. Comparing the four ligands, we expect catalysts with L = $P(OMe)_3$ to lead to polymer with the highest molecular weight. Indeed, the catalyst $[C_5Me_5CoHP(OMe)_3]^+$ is used in the living polymerization of ethylene.[22] Data comparing the molecular mass and degree of branching for polymer synthesized by a variety of late transition metal catalysts could corroborate our model once they become available.

If one compares the dynamics of wave packets starting from TS2, it is noticed that both lifetime and oscillation period τ_2 and T_2 of any particular ligand are now larger for the rhodium complexes (Table 2). This is a direct consequence of the much shallower potential around the ethyl minimum for the rhodium complexes (Figure 4), which is also reflected in values of

$$\Delta E_2 = E_{TS2} - E_{ethyl} \quad (10)$$

that are almost 50% lower than those for M = Co (see Table 1).

Among the four ligands, we observe the same trends as before, with the exception of the time constants for L = PH_3 no longer being the shortest in each series. The TS2 barrier for the associated complexes is significantly lower than those for all other ligands; this is likely due to sterical factors and leads to slower propagation in both the ethylene and ethyl regions of conformation space. The latter can be concluded using eq 9, because ΔE_2 for this ligand is lowered by 0.6−1.2 kcal/mol compared to the other ligands. Consequently, the lifetimes τ_2 and oscillation periods T_2 for both complexes are longer than that for, e.g., L = PF_3, although their masses are lowest in each case.

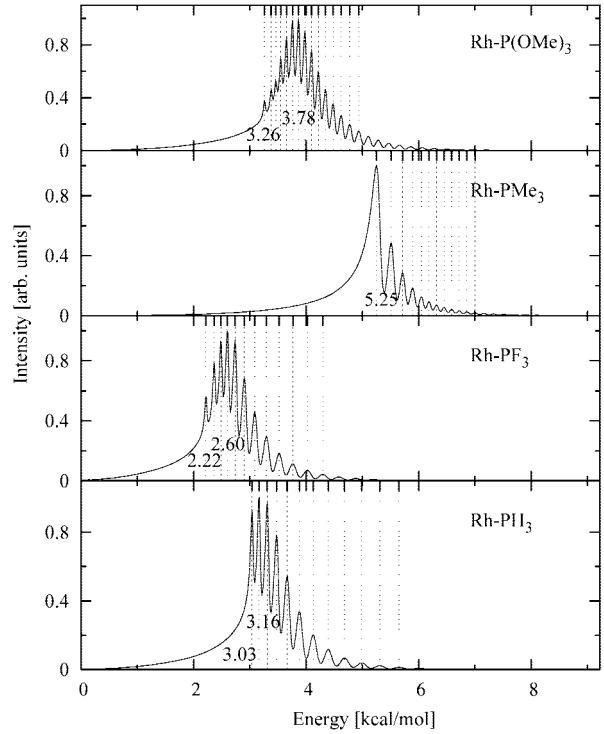

Figure 8. Calculated spectra for the $[CpRhLH(C_2H_4)]^+$ complexes. The vertical dashed lines represent the positions of the peaks as calculated by the filter diagonalization method. The numbers indicate the energies of the vibrational states with the lowest energy and maximum intensity, respectively.

4.3. Photoelectron Spectra. Using FFT, we calculated the PES of the studied complexes for the excitation of the neutral precursor to TS1/ES and plotted them in Figure 8 for the Rh complexes. The lowest energy eigenvalues are marked, and the positions of the highest peaks are also indicated. Energies, intensities, and lifetimes of the metastable vibrational states obtained by filter diagonalization for the agostic Rh complexes are given in Table 3.

Figure 8 shows that the positions of the peaks are well reproduced by filter diagonalization. The average energy difference $\overline{\Delta E}$ between two adjacent states also allows us to extract an oscillation period $\bar{T}$ according to

$$\overline{\Delta E} = 2\pi\hbar/\bar{T} \quad (11)$$

This compares well with that determined by tracing the position of the corresponding wave packet. For example, the oscillation period for the Rh−PF_3 complex is thus estimated to be 701 fs. This value is nearly the same as that found by tracing the wave packet (700 fs).

Compared to the corresponding values for the energy barriers and minima in Table 1, it is found that the lowest energy eigenvalue always lies a little above the agostic minimum and much lower than the energy barrier associated with TS1. For instance, for the Rh−$P(OMe)_3$ complex, the lowest energy eigenvalue is 3.26 kcal/mol. This value is slightly higher than the agostic energy of 3.14 kcal/mol and much lower than the TS1 barrier at 3.8 kcal/mol. This is reasonable and understandable, because the oscillation starts from TS1 and proceeds in the agostic minimum region. The wave packet thus samples the vibrational levels of the agostic structure, and the energy level mentioned above is the vibrational ground state. The peak with maximum intensity generally corresponds to the eigenvalue $E < E_{TS1}$ closest in energy to TS1. For example, for the Rh−PF_3

TABLE 3: Energies, *E*, Spectroscopic Intensities, *I*, and Lifetimes, τ_s, of the Metastable Vibrational States Obtained by Filter Diagonalization for the Complexes $[CpRhLH(C_2H_4)]^+$

L	*E* (kcal/mol)	*I* (arb units)	τ_s (fs)	L	*E* (kcal/mol)	*I* (arb units)	τ_s (fs)
PH_3	3.04	0.94	2131.6	PF_3	2.22	0.57	9307.9
	3.16	1.02	1002.5		2.36	0.79	3486.4
	3.31	0.98	478.6		2.49	0.94	1602.3
	3.47	0.78	247.9		2.60	1.01	725.7
	3.66	0.54	145.3		2.73	0.93	327.7
	3.88	0.34	103.2		2.90	0.69	199.9
	4.12	0.20	83.1		3.09	0.46	147.4
	4.39	0.12	71.5		3.29	0.30	111.3
	4.68	0.07	60.3		3.52	0.18	88.2
	4.98	0.04	49.5		3.76	0.11	77.1
	5.31	0.02	39.8		4.02	0.07	58.9
	5.65	0.01	33.0		4.30	0.04	52.8
	6.01	0.007	30.3		4.58	0.03	47.6
	6.37	0.004	30.1		4.88	0.02	42.8
PMe_3	5.25	1.00	119.4	$P(OMe)_3$	3.26	0.38	38756.8
	5.51	0.48	122.8		3.38	0.47	21215.1
	5.72	0.29	124.3		3.46	0.53	14332.5
	5.89	0.19	125.9		3.55	0.70	6040.4
	6.05	0.13	136.0		3.65	0.86	2991.5
	6.18	0.09	140.4		3.78	1.00	1490.9
	6.31	0.07	126.2		3.87	1.00	854.4
	6.45	0.06	122.0		3.98	0.91	540.2
	6.59	0.04	114.4		4.10	0.76	382.5
	6.72	0.03	110.2		4.22	0.60	300.9
	6.86	0.03	103.5		4.34	0.46	246.7
	7.00	0.02	88.0		4.47	0.35	207.9
	7.16	0.02	22		4.62	0.27	176.9
					4.78	0.20	149.5

complex, the energy eigenvalue closest to TS1 is at 2.60 kcal/mol, which is exactly where the highest peak is located. This is in accord with the FC principle, because the wave packet starts at TS1, and the highest probability for the wave packet appearing should therefore be close to the energy of TS1. The contrasting appearance of the spectrum for $Rh-PMe_3$ is due to its lack of an agostic minimum, and its PES peaks correspond therefore to resonances rather than metastable bound states.

From Table 3 it is seen that the filter diagonalization provides energies E_i that are practically identical to those from FFT. Additionally, the lifetimes τ_s of the metastable states are obtained. It is found that these lifetimes decrease with increasing excitation. In addition, we observe that these vibrational *state-specific* lifetimes exhibit a marked increase in the series

$$PMe_3 < PH_3 < PF_3 < P(OMe)_3$$

spanning a range of 2−3 orders of magnitude for the vibrational ground states of the agostic structures (119−39000 ps according to Table 3). This increase corresponds to the increase of the *broadband excitation* lifetimes τ_1 discussed in the previous subsection.

For those complexes with an agostic potential minimum, the *state-specific* lifetimes τ_s are due to a tuneling process, whereby a metastable vibrational eigenstate may decay although its energy is below E_{TS1}. The probability for this process is well-known to exponentially decrease with increasing mass and barrier height ΔE_1. As stated above, the latter quantity is negative for $L = PMe_3$, and the resonance lifetimes obtained for this ligand are therefore much shorter than the bound-state lifetimes for the other ligands.

It is seen that the τ_s values in our study correlate with the τ_1 for the various rhodium complexes and therefore provide an alternative method to qualitatively compare the ligands in terms of their stabilization of the complexes against β-elimination. This correlation is expected to hold unless ligands of similar mass but very different barrier heights are considered, since the lifetime τ_s *increases* with increasing ΔE_1. A prerequisite for this alternative method is the presence of metastable agostic vibrational states, i.e., of states that may decay by tuneling. This precludes the determination of values for τ_s for the cobalt complexes. Nevertheless, a qualitative ligand comparison from the PES is possible even for M = Co by a determination of the relative oscillation periods T_1 that can be obtained from spectral line spacings via eq 11.

5. Conclusions

The quantum dynamics of hydrogen elimination in cationic Co and Rh complexes has been studied theoretically, paying particular attention to the influence of the phosphine ligand L on the dynamics. The underlying potential energy data have been obtained from DFT calculations employing the BP86 functional; this was found in earlier work[5] to better reproduce the results of accurate coupled-cluster computations than the B3LYP hybrid functional.

The nuclear motion was computed at a quantum level by the method of wave packet propagation, and the effects of tunneling and zero-point energy were included. The initial wave packet was placed on either of the transition states TS1/ES or TS2, thus mimicking a broadband excitation from a neutral precursor complex. By suitable techniques (filtering, spectral quantization), state-specific spectroscopic intensities and lifetimes could then be extracted, which are independent of the initial wave packet location. Furthermore, the introduction of a CAP allows us to simulate the decay of the olefin−hydrido complex due to dissociation and, therefore, to calculate the lifetime of the complex due to β-elimination. The influence of the metal atom (Co or Rh) and a number of different ligands L on various time constants of the system, the periods of oscillation along the reaction coordinate, and the broadband and state-specific lifetimes were thus established for the first time. It was demonstrated that these parameters are correlated with the line spacing in the PES of these complexes, which would in principle permit a comparison of complex stabilities on the basis of spectroscopic data.

It turned out that an inclusion of ZPE had a significant influence on our results. In particular, the TS1 stationary points for most Co complexes, as well as the agostic minimum for the $Rh-PMe_3$ complex, are no longer identified on the ZPE-corrected reaction profile (Figures 3 and 4). This is a result of the comparatively small energy differences between the uncorrected TS1 and ethylene structures (less than 1 kcal/mol in the case of Co complexes) or TS1 and agostic structures (1−2 kcal/mol in the case of Rh complexes), which are of the same order of magnitude as the differences in the ZPE corrections for these structures.

We compared the ligand influence on complex stability using both transition state theory (TST) (section 3) and quantum dynamics (section 4). Both methods fortuitously agree in predicting Co complexes to be more stable against β-elimination than their Rh counterparts, but they lead to conflicting conclusions for the ligand trends. While TST favors ligands with a large ΔE_1 and, e.g., predicts the $Co-PF_3$ complex to be more stable against β-elimination than $Co-P(OMe)_3$, our wave packet propagation results reverse this finding. The increase of both

the broadband excitation lifetime τ_1 and the oscillation period T_1 with increasing mass of L and decreasing ΔE_1 (eq 9) indicates that ligands with a large mass and a shallow agostic minimum are most suitable to stabilize a late transition metal catalyst against β-elimination. Co−P(OMe)$_3$, the system with the greatest predicted stability, is indeed used as an ethylene polymerization catalyst. The state-specific lifetimes τ_s, on the other hand, generally increase with increasing mass and increasing values of ΔE_1 (see Tables 1 and 3). While both τ_1 and τ_s give the same trends for the four ligands examined, the latter depend on the tunnel effect and therefore predict a reduction in stability for complexes with an extremely shallow agostic minimum. Experimental data to confirm this are currently unavailable. In general, the mass of a ligand appears to have a greater influence on the reaction dynamics than its electronic properties.

We believe that our study provides conclusive evidence that the inclusion of quantum dynamical effects is necessary to accurately describe the reactivity of late transition metal catalysts for olefin polymerization, particularly when the influence of alternative ligands on the reaction is to be compared. With its exclusive focus on energetics, TST is unable to provide a comprehensive picture of this multistep process. It is hoped that these findings will encourage researchers active in the field of catalysis to appreciate wave packet propagation methods as a valuable tool for comparative studies. For example, a natural extension of the present work would consist in the inclusion of a broader variety of ligands in order to enhance its chemical significance. Our results indicate that ligands with an even higher mass might further stabilize the agostic state. This benefit could, however, be outweighed by the negative impact of higher transition-state energy barriers due to increased sterical hindrance if these ligands become bulkier as well. In particular, the height of the TS2 barrier is clearly correlated with ligand bulkiness. In passing, we note that the above considerations apply to both phosphine and Cp ligands, which is a likely reason why experimentalists prefer to use the more massive C_5Me_5 (Cp*); the computational demand for studies involving this ligand was found to be prohibitive.

Even more important, however, would be an investigation of the influence of dynamical effects on the thermal rate constants for the insertion/elimination process. We consider the current work to be a basis for a forthcoming study with this purpose that would enable a quantitative assessment of prospective catalysts. A theoretical framework is available for a direct and correct computation of rate constants beyond the widely used TST approach, incorporating tunneling as well as barrier recrossing effects on an equal footing.[52−54] It has already been applied successfully to small polyatomic systems.[55−57] Work along the directions outlined in this study is feasible that would permit the dynamical computation of such thermal rate constants, in addition to the processes studied here. This effort is currently ongoing in our group and already revealed substantial effects of tunneling on thermal rate constants and kinetic isotope effects.[58] Our forthcoming presentation of these results, which are beyond the scope of the present work, is likely to provide deeper insight into the various factors governing these important catalytic reaction steps. This is ultimately hoped to provide additional clues for an improved rational design of the corresponding catalysts.

Acknowledgment. This paper is dedicated to Professor Sason Shaik on the occasion of his 60th birthday. The authors are grateful to H. Wadepohl for helpful discussions, and to B. Schubert for providing his wave packet propagation program and helpful advice. This work has been supported by the *Deutsche Forschungsgemeinschaft* through *Sonderforschungsbereich 623* "Molekulare Katalysatoren: Struktur und Funktionsdesign".

References and Notes

(1) Johnson, L. K.; Killian, C. M.; Brookhart, M. *J. Am. Chem. Soc.* **1995**, *117*, 6414.
(2) Ittel, S. D.; Johnson, L. K.; Brookhart, M. *Chem. Rev.* **2000**, *100*, 1169.
(3) Shultz, L. H.; Tempel, D. J.; Brookhart, M. *J. Am. Chem. Soc.* **2001**, *123*, 11539.
(4) Chan, M. S. W.; Deng, L.; Ziegler, T. *Organometallics* **2000**, *19*, 2741.
(5) Bittner, M.; Köppel, H. *J. Phys. Chem. A* **2004**, *108*, 11116.
(6) Brookhart, M.; Green, M. L. *Organometallics* **1983**, *250*, 395.
(7) Brookhart, M.; Green, M. L.; Wong, L.-L. *Prog. Inorg. Chem.* **1988**, *36*, 1.
(8) Brookhart, M.; Lincoln, D. M.; Volpe, A. F.; Schmidt, G. F. *Organometallics* **1989**, *8*, 1212.
(9) Brookhart, M.; Hauptman, E.; Lincoln, D. M. *J. Am. Chem. Soc.* **1992**, *114*, 10394.
(10) Koga, K.; Morokuma, K. *Chem. Rev.* **1991**, *91*, 823.
(11) Musaev, D. G.; Morokuma, K. *Adv. Chem. Phys.* **1996**, *95*, 61.
(12) *Theoretical aspects of homogeneous catalysts. Applications of ab initio molecular orbital theory*; van Leeuwen, P. W., van Lenthe, J. H., Morokuma, K., Eds.; Kluwer Academic: Dordrecht, The Netherlands, 1994.
(13) Yoshida, S.; Sakaki, S.; Kobayashi, H. *Electronic processes in catalysis*; VCH Publishers: New York, 1992.
(14) Ziegler, T. *Chem. Rev.* **1991**, *91*, 651.
(15) Salahub, D. R.; Castro, M.; Fournier, R.; Calaminici, P.; Godbout, N.; Goursot, A.; Jamorski, C.; Kobayashi, H.; Martinez, A.; Papai, I.; Proynow, E.; Russo, N.; Sirois, S.; Ushio, J.; Vela, A. In *Theoretical and computational approaches to interface phenomena*; Sellers, H., Olab, J., Eds.; Plenum Press: New York, 1995; p 817.
(16) Siegbahn, P. E. *Adv. Chem. Phys.* **1996**, *93*, 333.
(17) *Transition metal hydrides*; Dedieu, A., Ed.; Wiley: New York, 1992.
(18) Niu, S.; Hall, M. B. *Chem. Rev.* **2000**, *100*, 353.
(19) Senn, H. M.; Blöchl, P. E.; Togni, A. *J. Am. Chem. Soc.* **2000**, *122*, 4098.
(20) Meier, R. J.; van Doremaele, G. H.; Ialori, S.; Buda, F. *J. Am. Chem. Soc.* **1994**, *116*, 7274.
(21) Bittner, M.; Köppel, H.; Gatti, F. *J. Phys. Chem. A* **2007**, *111*, 2407.
(22) Tanner, M. J.; Brookhart, M.; DeSimone, J. M. *J. Am. Chem. Soc.* **1997**, *119*, 7617.
(23) Parr, R. G.; Yang, W. *Density-functional theory of atoms and molecules*; Oxford University Press: Oxford, 1989.
(24) Becke, A. D. *Phys. Rev.* **1988**, *38*, 3098.
(25) Perdew, J. P. *Phys. Rev.* **1986**, *33*, 8822.
(26) Peng, C.; Schlegel, H. B. *Isr. J. Chem* **1993**, *33*, 449.
(27) Frisch, M. J.; Trucks, G. W.; Schlegel, H. B.; Scuseria, G. E.; Robb, M. A.; Cheeseman, J. R.; Montgomery, J. A., Jr.; Vreven, T.; Kudin, K. N.; Burant, J. C.; Millam, J. M.; Iyengar, S. S.; Tomasi, J.; Barone, V.; Mennucci, B.; Cossi, M.; Scalmani, G.; Rega, N.; Petersson, G. A.; Nakatsuji, H.; Hada, M.; Ehara, M.; Toyota, K.; Fukuda, R.; Hasegawa, J.; Ishida, M.; Nakajima, T.; Honda, Y.; Kitao, O.; Nakai, H.; Klene, M.; Li, X.; Knox, J. E.; Hratchian, H. P.; Cross, J. B.; Bakken, V.; Adamo, C.; Jaramillo, J.; Gomperts, R.; Stratmann, R. E.; Yazyev, O.; Austin, A. J.; Cammi, R.; Pomelli, C.; Ochterski, J. W.; Ayala, P. Y.; Morokuma, K.; Voth, G. A.; Salvador, P.; Dannenberg, J. J.; Zakrzewski, V. G.; Dapprich, S.; Daniels, A. D.; Strain, M. C.; Farkas, O.; Malick, D. K.; Rabuck, A. D.; Raghavachari, K.; Foresman, J. B.; Ortiz, J. V.; Cui, Q.; Baboul, A. G.; Clifford, S.; Cioslowski, J.; Stefanov, B. B.; Liu, G.; Liashenko, A.; Piskorz, P.; Komaromi, I.; Martin, R. L.; Fox, D. J.; Keith, T.; Al-Laham, M. A.; Peng, C. Y.; Nanayakkara, A.; Challacombe, M.; Gill, P. M. W.; Johnson, B.; Chen, W.; Wong, M. W.; Gonzalez, C.; Pople, J. A. *Gaussian03, Revision C.02*; Gaussian, Inc.: Wallingford, CT, 2003.
(28) Fukui, K.; Sato, S.; Fujimoto, H. *J. Am. Chem. Soc.* **1975**, *97*, 1.
(29) Fukui, K. *Adv. Chem. Phys.* **1981**, *14*, 363.
(30) Gonzalez, C.; Schlegel, H. B. *J. Phys. Chem.* **1989**, *90*, 2154.
(31) Gonzalez, C.; Schlegel, H. B. *J. Phys. Chem.* **1990**, *94*, 5523.
(32) Schork, R.; Köppel, H. *J. Phys. Chem.* **2001**, *115*, 7907.
(33) Mahapatra, S.; Köppel, H.; Cederbaum, L. S. *J. Phys. Chem.* **2001**, *105*, 2321.
(34) Somers, M. F.; Kingma, S. M.; Pijper, E.; Kroes, G. J.; Lemoine, D. *Chem. Phys. Lett.* **2002**, *360*, 390.
(35) Zhang, J. Z. *Theory and application of quantum molecular dynamics*; World Scientific: River Edge, NJ, 1999.
(36) Neuhauser, D.; Baer, M. *J. Phys. Chem.* **1989**, *91*, 4651.
(37) Vibók, Á.; Balint-Kurti, G. G. *J. Phys. Chem.* **1992**, *96*, 7615.
(38) Vibók, Á.; Balint-Kurti, G. G. *J. Phys. Chem.* **1992**, *96*, 8712.
(39) Riss, U. V.; Meyer, H.-D. *J. Chem. Phys.* **1996**, *105*, 1409.

(40) Arnoldi, W. E. *Appl. Math.* **1951**, *9*, 17.
(41) Saad, Y. *Lin. Alg. Appl.* **1980**, *24*, 269.
(42) Schinke, R. *Photodissociation dynamics*; Cambridge University Press: Cambridge, 1993.
(43) Neuhauser, D. *J. Phys. Chem.* **1990**, *93*, 2611.
(44) Neuhauser, D. *J. Phys. Chem.* **1993**, *100*, 5076.
(45) Wall, M. R.; Neuhauser, D. *J. Phys. Chem.* **1995**, *102*, 8011.
(46) Mandelshtam, V. A.; Taylor, H. S. *J. Phys. Chem.* **1997**, *107*, 6756.
(47) Zeller, A.; Strassner, T. *Organometallics* **2002**, *21*, 4950.
(48) Wadepohl, H.; Köppel, H.; et al. To be published.
(49) Assion, A.; Baumert, T.; Bergt, M.; Brixner, T.; Kiefer, B.; Seyfried, V.; Strehle, M.; Gerber, G. *Science* **1998**, *282*, 919.
(50) Vogt, G.; Krampert, G.; Niklaus, P.; Nuernberger, P.; Gerber, G. *Phys. Rev. Lett.* **2005**, *94*, 6.
(51) Brixner, T.; Krampert, G.; Pfeifer, T.; Selle, R.; Gerber, G.; Wollenhaupt, M.; Graefe, O.; Horn, C.; Liese, D.; Baumert, T. *Phys. Rev. Lett.* **2004**, *92*, 20.
(52) Miller, W. H.; Schwartz, S. D.; Tromp, J. W. *J. Chem. Phys.* **1983**, *79*, 4889.
(53) Miller, W. H. *J. Phys. Chem. A* **1998**, *102*, 793.
(54) Manthe, U. *J. TC. Chem.* **2002**, *1*, 153.
(55) Lasorne, B.; Gatti, F.; Baloitcha, E.; Meyer, H.-D.; Desouter-Lecomte, M. *J. Chem. Phys.* **2004**, *121*, 644.
(56) van Harrevelt, R.; Honkala, K. N.; Nøskov, J. K.; Manthe, U. *J. Chem. Phys.* **2005**, *122*, 234702.
(57) Wu, T.; Werner, H.-J.; Manthe, U. *Science* **2004**, *306*, 2227.
(58) Klatt, G.; Köppel, H. To be published.

JP807676N